TECHNIQUES

Mouse redox histology using genetically encoded probes

Yuuta Fujikawa,¹*† Leticia P. Roma,¹* Mirko C. Sobotta,¹ Adam J. Rose,² Mauricio Berriel Diaz,^{2,3} Giuseppe Locatelli,⁴ Michael O. Breckwoldt,^{4,5‡} Thomas Misgeld,^{5,6,7} Martin Kerschensteiner,^{4,6} Stephan Herzig,^{2,3} Karin Müller-Decker,⁸ Tobias P. Dick^{1§}

Mapping the in vivo distribution of endogenous oxidants in animal tissues is of substantial biomedical interest. Numerous health-related factors, including diet, physical activity, infection, aging, toxins, or pharmacological intervention, may cause redox changes. Tools are needed to pinpoint redox state changes to particular organs, tissues, cell types, and subcellular organelles. We describe a procedure that preserves the in vivo redox state of genetically encoded redox biosensors within histological tissue sections, thus providing "redox maps" for any tissue and comparison of interest. We demonstrate the utility of the technique by visualizing endogenous redox differences and changes in the context of tumor growth, inflammation, embryonic development, and nutrient starvation.

INTRODUCTION

Endogenously produced reactive oxygen species (ROS) are widely believed to play an important role in health and disease. One species of particular interest is hydrogen peroxide (H₂O₂), which is traditionally implicated in "oxidative stress" but also plays a role in physiological signal transduction (1). H₂O₂ emitted from mitochondria may be a signal that links mild mitochondrial dysfunction (as may occur during physical exercise or calorie restriction) to health benefits, through the induction of cytoprotective pathways, a concept now known as "mitohormesis" (2, 3). The main mechanism by which H₂O₂ modulates cellular behavior is through selective protein thiol oxidation, which is antagonized by the NADPH (reduced form of nicotinamide adenine dinucleotide phosphate) dependent thiol reducing systems. Glutathione (GSH) is the dominant lowmolecular weight thiol in mammalian cells. Differences or changes in the extent of GSH oxidation are considered to indicate shifts in endogenous "redox balance." The development of genetically encoded fluorescent probes for H_2O_2 (4, 5) and for the GSH redox potential (E_{GSH}) (6) represents a major advance that enabled analysis of subcellular compartmentspecific real-time information from within living cells and from whole organisms (7, 8). Compartmental localization and chemical specificity of redox sensors are crucial for obtaining meaningful insights from redox measurements (9, 10).

¹Division of Redox Regulation, DKFZ–ZMBH (German Cancer Research Center–Center for Molecular Biology of the University of Heidelberg) Alliance, DKFZ, Im Neuenheimer Feld 280, 69120 Heidelberg, Germany. ²Joint Division Molecular Metabolic Control, DKFZ-ZMBH Alliance, DKFZ Heidelberg, Center for Molecular Biology (ZMBH) and University Hospital, University of Heidelberg, 69120 Heidelberg, Germany. ³Institute for Diabetes and Cancer (IDC) and Joint Heidelberg–IDC Translational Diabetes Program, Heidelberg University Hospital, Helmholtz Center Munich, 85764 Neuherberg, Germany. ⁴Institute of Clinical Neuroimmunology, Ludwig-Maximilians-Universität München, 81377 Munich, Germany. ⁵Institute of Neuronal Cell Biology, Technical University of Munich, 80802 Munich, Germany. ⁶Munich Cluster for Systems Neurology (SyNergy), 81377 Munich, Germany. ⁷German Center for Neurodegenerative Diseases (DZNE), 81377 Munich, Germany. ⁸Core Facility Tumor Models, DKFZ, 69120 Heidelberg, Germany.

*These authors contributed equally to this work.

†Present address: School of Life Sciences, Tokyo University of Pharmacy and Life Sciences, 1432-1 Horinouchi, Hachioji, Tokyo 192-0392, Japan. ‡Present address: Department of Neuroradiology, University of Heidelberg, Im Neuenheimer Feld 400, 69120 Heidelberg, Germany.

§Corresponding author. E-mail: t.dick@dkfz.de

The use of fluorescent proteins transgenically expressed in multicellular organisms is limited by optical accessibility. Consequently, transgenic redox reporters have been primarily used in model animals that are either small or translucent or both (7, 11, 12). For mice, direct in vivo imaging with fluorescent biosensors is limited to superficial tissues or to those tissues that can be accessed by surgical intervention (8). Thus, redox imaging methods are needed that are more broadly applicable to mouse studies. For example, commonly encountered questions include whether genetic alterations, infections, aging, exercise, changes in diet, toxins, or pharmacological treatments lead to redox changes in vivo. It is imperative to discover within which organs, tissues, cell types, and subcellular organelles these redox changes occur. Hence, we looked for a procedure that preserves the endogenous state of genetically encoded redox probes in the context of histological tissue sections, thus providing sectional "redox maps" for any organ or tissue of interest. This approach would be limited to providing "snapshots" at selected time points but enables the comparison of the effect of many conditions or treatments on redox status in most mouse models and in most tissues with subcellular resolution.

We present a procedure that enables the preservation and visualization of the redox state of an expressed biosensor in mouse tissue sections. We demonstrate the method with tissue sections from mice expressing a mitochondrially targeted fusion protein of redox-sensitive green fluorescent protein 2 and the oxidant receptor peroxidase 1 (mito-roGFP2-Orp1), which is an H₂O₂ biosensor (4), or a mitochondrially targeted fusion protein of glutaredoxin 1 and redox-sensitive green fluorescent protein 2 (mito-Grx1-roGFP2), which is a biosensor for E_{GSH} (6). In this procedure, cryogenic tissue sections are exposed to a chemical that maintains the redox state of the expressed biosensors by protecting them from oxidation by atmospheric oxygen, fixatives, or other influences. Briefly, the organ of interest is snap-frozen and cryosectioned, and the sections are immediately immersed in N-ethylmaleimide (NEM), a fast-acting membranepermeable alkylating agent, to clamp the redox state of roGFP2 within the cryosection. Alkylation rapidly and irreversibly traps reduced biosensor molecules in the reduced state, preventing ex vivo oxidation by atmospheric oxygen or paraformaldehyde (PFA) treatment, thus enabling subsequent fixation and storage. The process of cryogenic followed by chemical preservation effectively prevented probe oxidation and preserved reduced tissues in their reduced state. We introduced roGFP2-based redox probes into mice by three different means: tumor

xenografting, adenoviral gene transfer, and transgenesis. To illustrate the usefulness and scope of the approach, we assessed redox differences within tumor tissues, redox changes that occur during embryonic development, and redox changes caused by inflammation or nutrient starvation.

RESULTS

Redox imaging of xenografted tumors

To validate the cryogenic chemical probe preservation technique (Fig. 1A), we first used a tumor xenograft model. We established a human non-small cell lung cancer cell line (H1975) stably expressing the mitochondrial H₂O₂ biosensor mito-roGFP2-Orp1 (4). The Orp1 domain facilitates roGFP2 oxidation in the presence of H₂O₂ (Fig. 1B); thus, the ratio of oxidized to reduced roGFP2 is a function of H₂O₂ concentration, which changes fluorescence emission. We confirmed proper mitochondrial localization (Fig. 2A) and dynamic responsiveness to either exogenous (Fig. 2B) or endogenous oxidants (Fig. 2C) as induced by respiratory chain inhibitors (rotenone or antimycin A) in the H1975 cells. We showed that pretreatment of the cultured cells with NEM prevented PFA-induced oxidation of the biosensor (Fig. 2, D and E). Athymic nude mice injected subcutaneously with the mito-roGFP2-Orp1-expressing H1975 cells developed tumors, which we harvested, snap-froze with liquid nitrogen, and cryosectioned. Treatment of sections with the oxidant diamide (DA) or the reductant dithiothreitol (DTT) before exposure to NEM confirmed that the 405/488-nm fluorescence ratio increased upon DA treatment and decreased upon DTT treatment (fig. S1, A and B). The ratio difference between the fully oxidized (DA treatment) and fully reduced (DTT treatment) samples defined the dynamic range of the biosensor in the tissue (fig. S1B). Using the cryogenic chemical preservation protocol, we mapped the relative degree of probe oxidation (OxD_{roGFP2}) in different regions of the tumor mass (Fig. 2F). The necrotic core (Fig. 2, F and G, iii), identified by low nuclear density in hematoxylin and eosin stained serial sections, exhibited almost full probe oxidation. In the nonnecrotic regions, the roGFP2 redox state was heterogeneous, ranging from almost completely reduced to fully oxidized (Fig. 2, F and G, i and ii). These differences may arise from clonal or metabolic heterogeneity within the tumor mass, possibly associated with differences in oxygen or nutrient availability.

Comparison of the biosensor redox state in tissue sections prepared with or without NEM (the chemical step of the cryochemical protocol) before fixation with PFA showed that without the NEM step, PFA partially oxidized the biosensor (Fig. 2, H and I). As expected, the biosensor remained in the oxidized state in highly oxidized intratumoral regions regardless of NEM treatment (Fig. 2, H and I). Thus, NEM treatment of the sections prevented PFA-induced probe oxidation.

Redox imaging of mouse liver after adenovirus-mediated probe transduction

Next, we used adenovirus-mediated gene transfer through tail vein injection to express the mito-roGFP2-Orp1 biosensor in the liver. Proper mito-chondrial localization of the biosensor (fig. S2A), responsiveness of the biosensor to complete oxidation by DA and complete reduction by DTT (fig. S2, B and C), and preservation of biosensor redox state by NEM treatment (fig. S2, D and E) were confirmed in liver tissue sections. To investigate the influence of liver inflammation on the mitochondrial probe redox state, we injected mice with either tumor necrosis factor— α (TNF α), lipo-

polysaccharide, or concanavalin A and compared the redox state of the biosensor to the control condition of phosphate-buffered saline (PBS) injection. All three inflammatory compounds produced heterogeneous effects with increased biosensor oxidation in a sparse population of cells (Fig. 3A), correlating with limited signs of liver damage at the time of analysis (fig. S3A). On the basis of the fluorescence ratio measured in individual cells (fig. S3B), we calculated OxD_{ToGFP2} (Fig. 3B), which revealed substantial probe oxidation in individual cells within the population.

To demonstrate the possibility of combining redox probe measurements with conventional immunohistochemistry, we stained representative cryogenic chemical-preserved and PFA-fixed sections from mice injected with TNFα with an antibody against complement receptor type 3 (CD11b), a protein present on phagocytes in a clustered pattern. Although not every cell in the tissue will be infected with the virus encoding the biosensor, we expect that both the hepatocytes and the macrophages can be infected with the virus and express the biosensor. Indeed, we observed regions of biosensor oxidation that colocalized with CD11b staining, implicating macrophages as a source of H₂O₂ (Fig. 3, C and D). These results showed that the NEM preservation

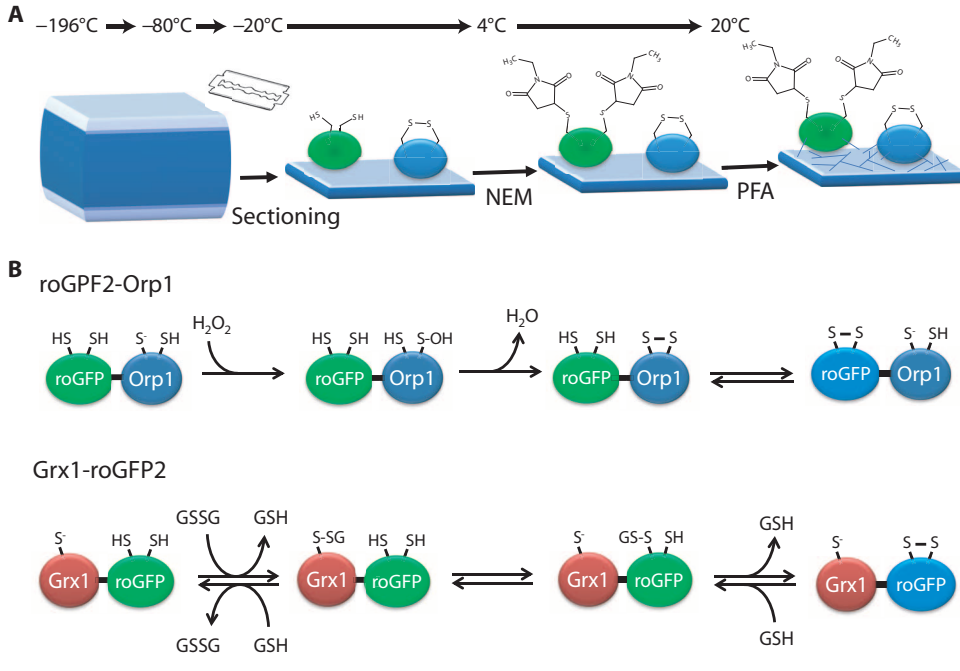
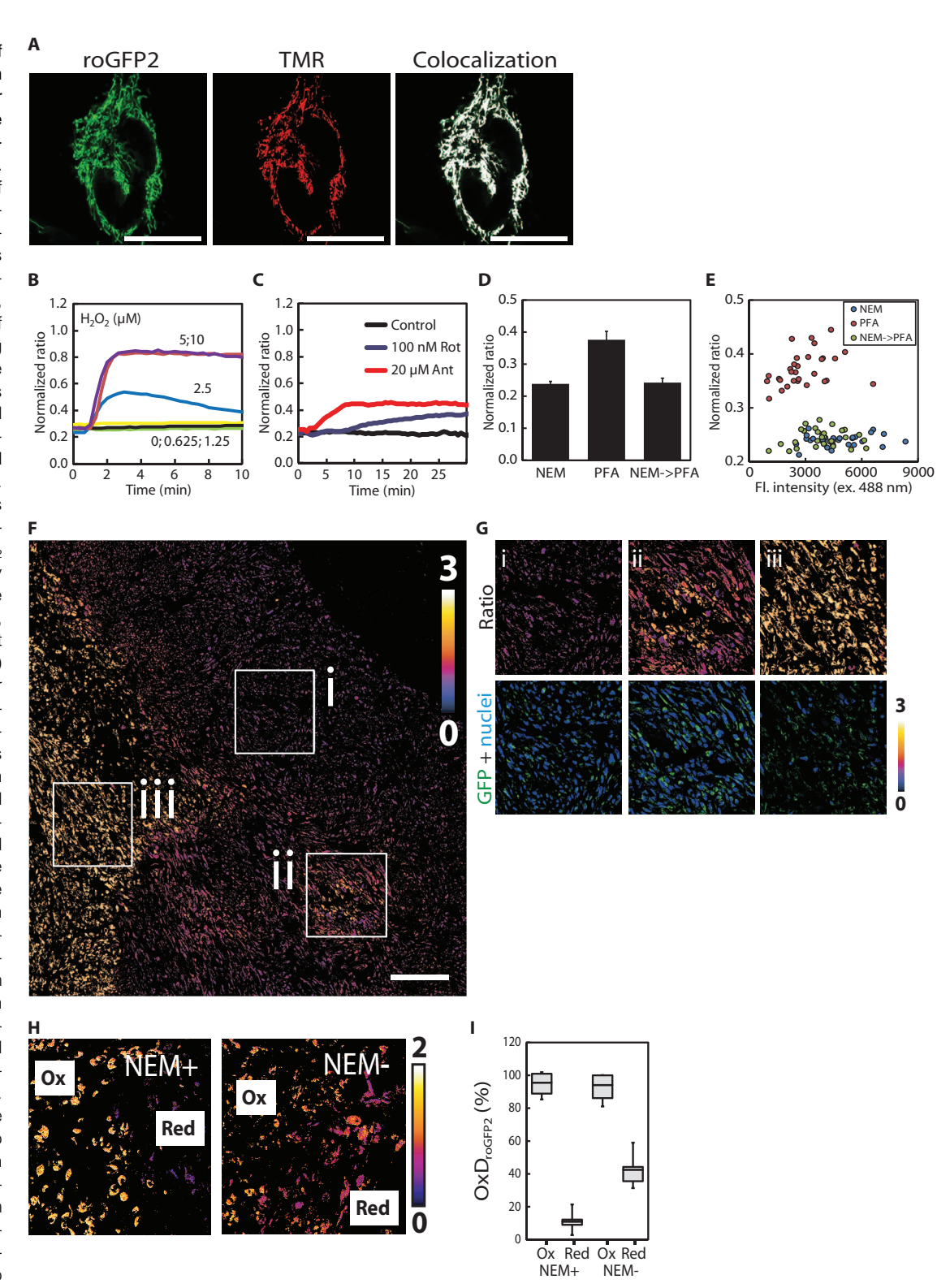
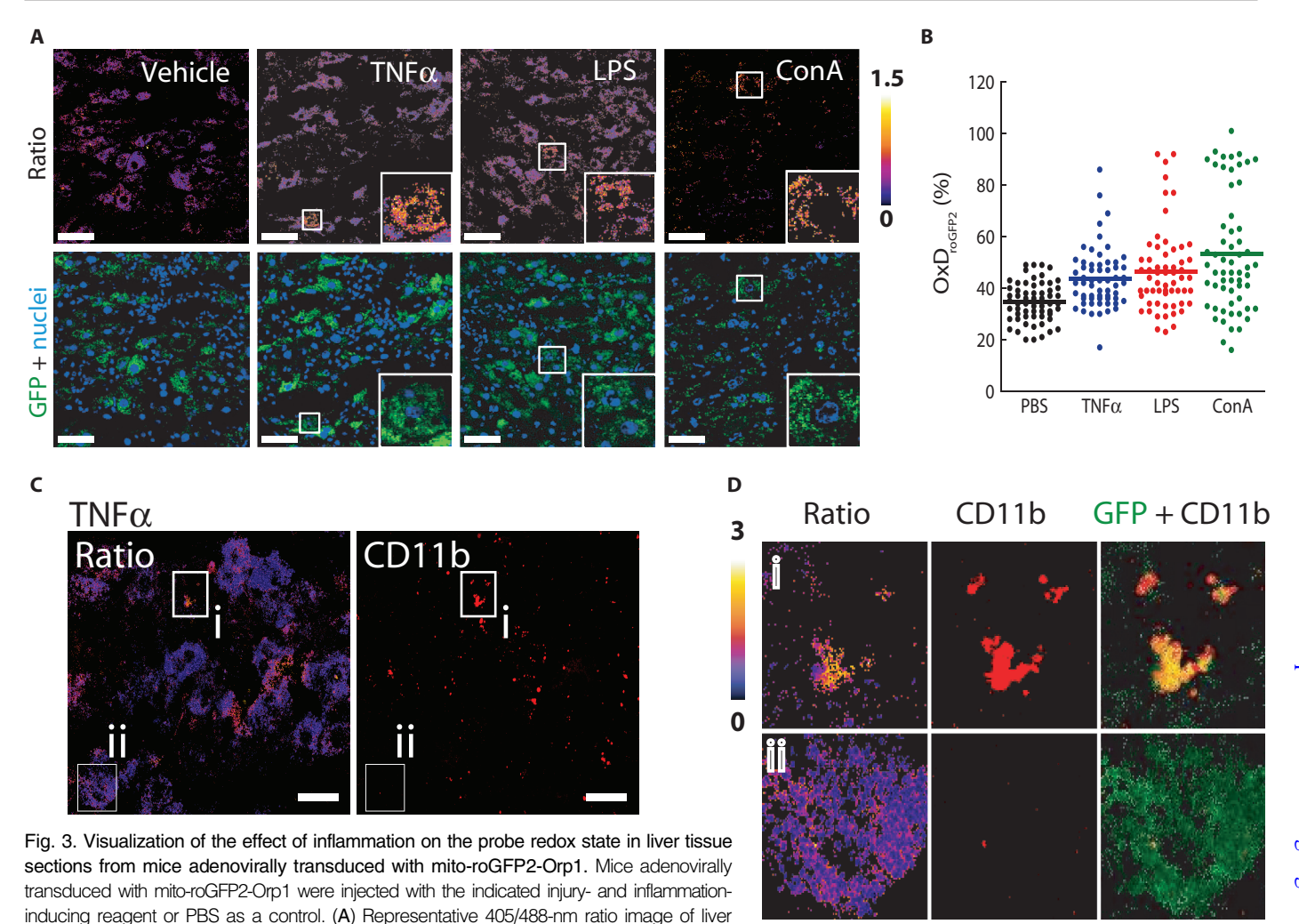


Fig. 1. Probe conservation strategy and mechanisms of redox sensing. (A) Cryopreserved organs are cryosectioned, and sections were immediately treated with the fast-acting thiol blocker NEM to exclude artificial roGFP2 thiol oxidation during tissue fixation with PFA. (B) The roGFP2 biosensors and their mechanism of detecting redox status. The top shows how H_2O_2 triggers the oxidation of roGFP2 through mediation by the thiol peroxidase Orp1. The bottom shows how oxidized GSH (GSSG) triggers the oxidation of roGFP2 through mediation by the glutaredoxin Grx1.

Fig. 2. Visualization of probe redox state in H1975 cells and tumor tissue sections of these cells expressing the mitoroGFP2-Orp1 biosensor. (A) Colocalization of roGFP2 and tetramethylrhodamine (TMR) fluorescence in H1975 cells stably expressing mitoroGFP2-Orp1. Scale bars, 40 μm. (B) Response of H1975 cells expressing mito-roGFP2-Orp1 to the indicated concentrations of H₂O₂. The 0, 0.625, and 1.25 µM conditions are overlapping, and the 5 and $10 \mu M$ conditions are overlapping. (C) Response of H1975 cells expressing mito-roGFP2-Orp1 to endogenous H₂O₂ as induced by respiratory chain inhibitors rotenone (Rot) and antimycin A (Ant), added 30 s after the start of the measurement. (D) Redox state of the biosensor in cells exposed to the indicated chemicals in the indicated order. Error bars represent SD of the mean (n = 3, 10 cells analyzed)per sample). (E) Relationship between measured biosensor fluorescence ratios and fluorescence intensity (Fl. intensity) in individual cells used to calculate data in (D). (F) Representative 405/488-nm ratio image of a section from a cryogenic chemically preserved and PFA-fixed tumor of H1975 cells expressing mito-roGFP2-Orp1. (G) Enlarged views of the regions indicated in (F) to illustrate the variation in probe redox status in the tissue. Top panels: 405/488-nm ratio images; bottom panels: nuclei (blue) and GFP fluorescence (green). (H) Ratio images of PFA-fixed cryo-



sections with and without NEM pretreatment. "Ox" and "Red" indicate fully oxidized and reduced regions, respectively. Bar, 50 µm. (I) Degree of probe oxidation (based on five sections derived from three different tumors) in regions Ox and Red like those shown in (H). Boxes, lower/upper quartile; whiskers, 5th/95th percentile.



sections. Top panels: 405/488-nm ratio images; bottom panels: nuclei (blue) plus GFP (green). Inset: Enlarged view of a region with highly oxidized cells. LPS, lipopolysaccharide; ConA, concanavalin A. (B) Dot plot representing the degree of probe oxidation (n = 60 cells, from two animals, 30 cells per animal and treatment). Bar indicates mean. (C) Representative images of liver sections from TNF α -injected mice showing the redox state of the biosensor [405/488-nm ratio (left panel)] and CD11b antibody staining of the same section (right panel) (n = 3). Scale bars, 30 μ m. (D) Enlarged view of the indicated regions in (C) showing the roGFP2 405/488-nm fluorescence ratio (left panels), CD11b staining (middle panels), and merged images of roGFP2 fluorescence (green) and CD11b staining (red).

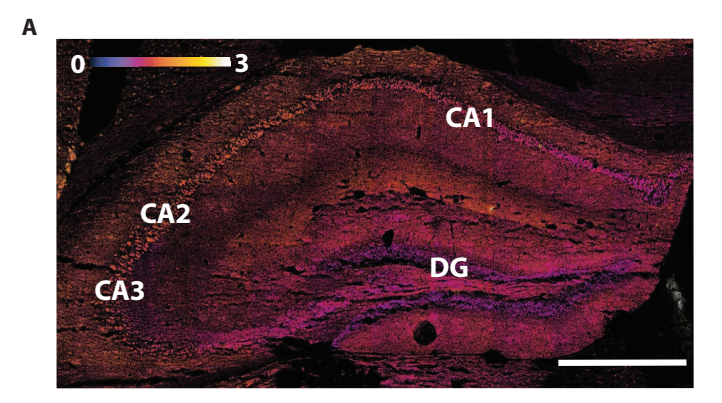
step is compatible with at least some antibodies and thus can be combined with immunohistochemistry.

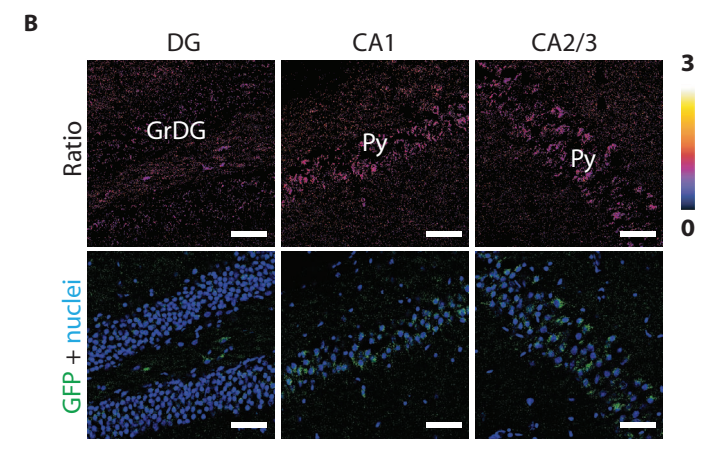
Redox imaging of brain and embryonic tissues from biosensor transgenic mice

We applied the cryogenic chemical preservation method to analyze deep solid tissues from biosensor transgenic mice. We used transgenic mice expressing a mitochondrial $E_{\rm GSH}$ probe (6) under a neuron-specific promoter (Thy1-mito-Grx1-roGFP2), as previously characterized and used for in vivo two-photon imaging of the spinal cord (8). Similar to the $\rm H_2O_2$ biosensor, the mito-Grx1-roGFP2 probe localizes to the mitochondria and uses roGFP2 as the fluorescent reporter. In this case however, the attached Grx1 moiety catalyzes the redox equilibration between roGFP2 and GSH, thus yielding a measure of $E_{\rm GSH}$ (Fig. 1B). After confirming that the cryogenic chemical preservation method was effective with this biosensor in this tissue (fig. S4, A to D), we examined the $\rm OxD_{roGFP2}$ status in hippocampal sections. Ratiometric imaging of cryogenic chemically preserved hippocampus

sections revealed that dentate gyrus (GD) granule cells are associated with a more reducing $E_{\rm GSH}$ than pyramidal cells in the cornu ammonis 1 (CA1), CA2, and CA3 regions (Fig. 4, A to C).

We also generated mice expressing the H_2O_2 probe mito-roGFP2-Orp1 globally (ROSA26/CAG-stop fl -mito-roGFP2-Orp1 × CMV-Cre). The cryogenic chemical preservation method preserved the status of the biosensor in reduced tissues, as exemplified for choroid plexus brain sections (Fig. 5, A and B), and prevented biosensor oxidation within liver tissue sections (Fig. 5C). We used this globally expressed biosensor to evaluate the redox status of tissues in early embryos. Because of the small diameter of early embryos, we treated the whole embryos sequentially with NEM and PFA before cryosectioning. We detected globular regions of increased biosensor oxidation in the livers of E12.5 (embryonic day 12.5) embryos (Fig. 5D and fig. S5). These regions likely represent clusters of proliferating or differentiating cells because both hematopoietic stem cell differentiation and hepatocyte proliferation are suggested to involve increased production of H_2O_2 (13–15).





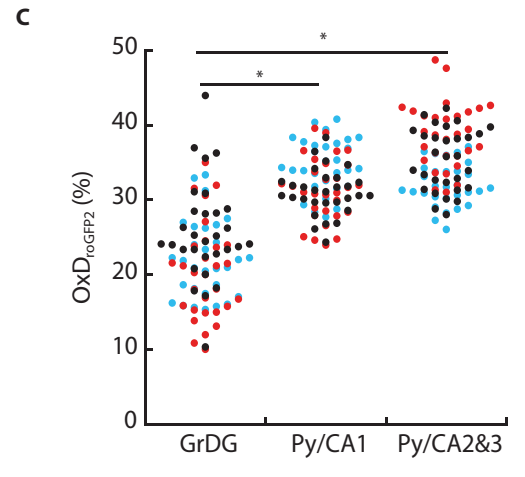


Fig. 4. Visualization of redox status in hippocampus of mice using the mito-Grx1-roGFP2 biosensor. (A) Representative 405/488-nm ratio image of the coronal hippocampus from *thy1*-mito-Grx1-roGFP2 transgenic mice. The granule cell layer of dentate gyrus (DG) and pyramidal cell regions CA1 to CA3 are indicated. Scale bar, 500 μ m. (B) Representative ratio (top panels) and fluorescence images [bottom panels, GFP (green) plus nuclei (blue)] of different hippocampal regions. GrDG, granule cell layer of DG; Py, pyramidal cell region. Scale bars, 50 μ m. (C) Dot plot representing the percent of probe oxidation in individual cells (three animals, 30 cells per region and animal). Different colors represent different mice. Statistical analysis was conducted by paired Student's *t* test: GrDG versus Py/CA1, *P < 0.05; GrDG versus Py/CA2&3, *P < 0.05.

With adult mito-roGFP2-Orp1 transgenic mice, we also compared muscle tissues from fed and starved animals using the cryogenic chemical preservation method. Starvation increased the oxidation of the biosensor (Fig. 5, E and F, and fig. S6, A and B), consistent with the enhanced fatty acid oxidation (16) that occurs under these conditions and with the suggestion that starvation-induced oxidants trigger autophagy, thus leading to skeletal muscle atrophy during nutrient deprivation (17). In muscle sections from starved mice, oxidative and glycolytic muscular fibers (as differentiated by mitochondrial content) exhibited comparatively high and low probe oxidation, respectively (Fig. 5, G and H, and fig. S6, C and D).

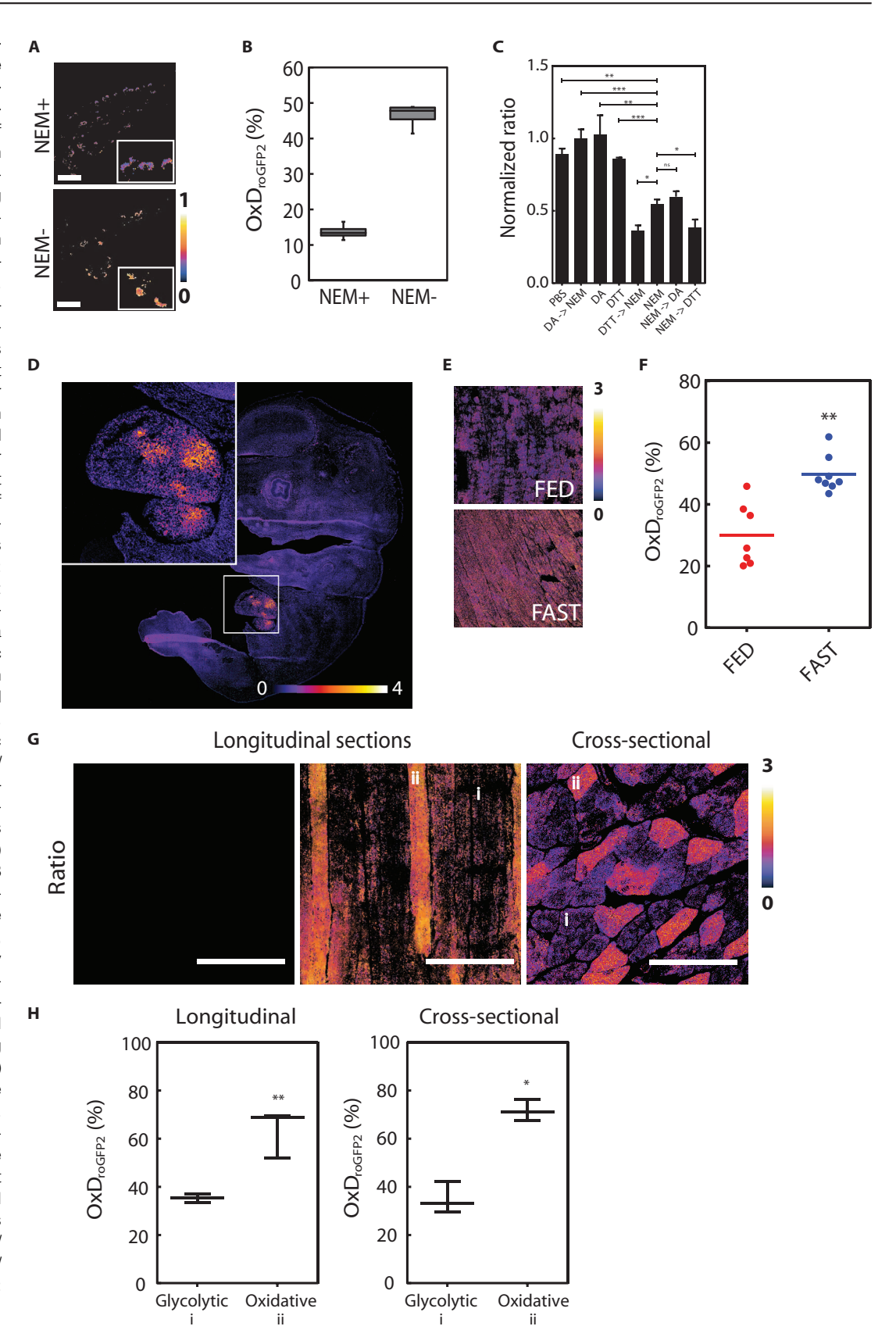
DISCUSSION

The widespread application of genetically encoded fluorescent redox probes to mouse preclinical models has been limited because most organs and tissues are not optically accessible in the living organism. Here, we showed that a simple chemical exposure procedure can be combined with cryosectioning to preserve the redox state of the genetically encoded biosensor and, thus, reveal the spatial distribution of probe redox states in tissue sections from mice (or xenotransplantated tumors) expressing roGFP2-based redox biosensors. The chemical preservation step involves exposing the cryosectioned tissue samples to the membrane-permeable thiol-alkylating agent NEM, which combines several favorable properties. First, NEM by itself does not interfere with roGFP2 fluorescence measurements, neither in the unconjugated nor in the roGFP2-conjugated state (6). Second, NEM protects the reduced probe from oxidation by irreversibly alkylating the roGFP2 cysteines, thus locking any reduced roGFP2 in the disulfide-free state. Third, NEM treatment additionally protects against reduction of oxidized roGFP2 because NEM generally alkylates free thiols, thus preventing reduction of oxidized roGFP2 by disulfide exchange with thiols contained within the tissue section. Fourth, NEM penetrates tissues rapidly and efficiently, especially when applied to thin sections that are only a few cell layers in diameter. The sections become alkylated very rapidly due to short diffusion distances and simultaneous exposure to NEM from both sides.

The roGFP2 disulfide can still be reduced within the NEM-treated section if a sufficiently large excess of reductant (for example, DTT) is applied, because the exogenous reductant will penetrate the section, consume any remaining free NEM, and then reduce any disulfide bonds (including those in roGFP2). However, this is neither a concern nor relevant to our procedure because reductive equivalents will not spontaneously reemerge within NEM-treated tissue sections unless an exogenous reductant is applied. In our hands, NEM-treated and PFA-fixed tissue sections did not show changes in the roGFP2 fluorescence ratio when stored at -80° C for prolonged periods of time.

We also showed that roGFP2 fluorescence imaging can be combined with conventional immunohistochemistry, thus expanding the scope of the technique and potentially enabling the identification of specific cell types associated with oxidative changes. In principle, antibody binding to a cysteine-containing epitope could be lost after modification of the epitope by NEM; thus, each epitope-antibody combination will need to be empirically tested. However, we anticipate that such loss of epitope recognition is the exception. Although we have only used mitochondrially targeted probes in this study, the procedure should equally apply to roGFP2-based biosensors targeted to other compartments (including the cytosol), as long as they provide a sufficient signal-to-noise ratio. A specific advantage of roGFP2-based probes is their ratiometric insensitivity to pH changes (10), which is a major drawback for any probe on the basis of circularly permuted fluorescent proteins (18–20). At present, chemical probes do not offer the

Fig. 5. Histological redox imaging of embryos and muscle tissue from adult mice expressing the mito-roGFP2-Orp1 biosensor. (A) Effect of NEM on probe oxidation in choroid plexus. Representative ratio images showing PFA-fixed choroid plexus endothelial cells prepared with or without prior NEM treatment. Scale bars, 50 µm. The inset shows an enlargement. (B) Percent probe oxidation in choroid plexus sections with or without NEM treatment (n = 3). Boxes, lower/upper quartile; whiskers, 5th/95th percentile. (C) Normalized 405/488-nm ratio of adult liver sections treated with different combinations and order of DA, DTT, and NEM as indicated (n = 3). Arrow means "followed by." Student's t test: ***P < 0.001, **P < 0.01, *P < 0.05; ns, not significant. (D) Representative ratio image of a mito-roGFP2-Orp1 transgenic E12.5 embryo preserved with NEM before PFA fixation and cryogenic sectioning (n = 9). The inset shows the embryonic liver. (E) Representative 405/ 488-nm ratio images of mitoroGFP2-Orp1 transgenic gastrocnemius and soleus muscles after 24 hours of feeding (FED) or fasting (FAST) (n = 7 to 8 animals per group). (F) Fastingrelated changes in the degree of probe oxidation. **P < 0.01, Student's t test followed by Welch's correction test. (G) Representative ratio images of longitudinal and cross-sectional muscle sections. Mice lacking sensor expression (left panel) were used as autofluorescence controls. Scale bars, 100 µm. n = 3 to 4 animals. (i) and (ii) indicate glycolytic and oxidative fibers, respectively. (H) Percent probe oxidation in longitudinal and cross sections. Error bars represent SEM. Boxes, lower/ upper quartile; whiskers, 5th/ 95th percentile. Student's t test: **P < 0.01, *P < 0.05.



combination of advantageous properties integral to genetically encoded probes. Moreover, in vivo applications of chemical probes often suffer from pharmacokinetic constraints and may give rise to artifacts by tissue-or cell type–specific differences in uptake or export.

Limitations that generally apply to genetically encoded reporters also apply to the redox probes used in this study (10, 21). We mention one potentially important limitation in the context of histological redox imaging, which is probe sensitivity. The H₂O₂-sensitive probe roGFP2-Orp1 is of similar sensitivity as the HyPer probe (4) but is less sensitive than peroxiredoxin-2, which is one of the most H₂O₂-sensitive proteins in mammalian cells (22). As shown here and elsewhere (7), numerous phenomena, related to both stress and signaling situations, can be detected with the roGFP2-Orp1 biosensor. Yet, detection of the slightest (metabolic) H₂O₂ fluctuations, close to the steady-state baseline, presumably taking place in the low nanomolar or even picomolar range, will probably require the development of peroxiredoxin-based redox probes. Peroxiredoxins are increasingly recognized to engage in redox signaling relays (23) and therefore should also be able to communicate their redox state to roGFPs. In any case, the protocol described herein will also apply to future probes operating on the basis of roGFP2.

In summary, the key advantages of genetically encoded redox probes, namely, precise cellular and subcellular targetability, chemical specificity, and ratiometric measurement, are made available to a broad range of histological studies. The chemical conservation approach should be applicable to investigate the occurrence of redox differences and changes under various physiological and pathological conditions. For example, it is often suggested that most cancer cells exhibit increased endogenous ROS generation, leading to either increased steady-state levels or increased turnover of ROS. This has led to the idea that drugs that further enhance ROS generation (or selectively inhibit reducing systems) will push tumor cells over their tolerable threshold of oxidative stress, thus triggering selective cell death (24). However, in previous intervention studies, it remained mostly unknown to which extent drugs actually reached different parts of a tumor, to which extent redox changes were actually inflicted in situ, and to which extent tumor cells responded differently relative to the surrounding healthy tissues. Histological redox imaging should enable the reliable investigation of how tumors and their surroundings respond to prooxidative or antireductive drugs, alone, or in combination with conventional radio- or chemotherapy. It will also be of interest to study the redox response of healthy and tumor tissues to compounds presumed to act as "antioxidants," given recent findings suggesting that such compounds may accelerate tumor progression and promote metastasis (25-27).

MATERIALS AND METHODS

Cell culture

Phoenix-AMPHO and human embryonic kidney–293 cells were grown in Dulbecco's modified Eagle medium (Invitrogen). H1975 non–small cell lung carcinoma cells (obtained from American Type Culture Collection) were grown in RPMI 1640 (Invitrogen). Media were supplemented with 10% heat-inactivated fetal bovine serum (FBS) (Invitrogen), 2 mM L-glutamine (Invitrogen), penicillin (100 U/ml), and streptomycin (100 mg/ml) (Invitrogen). Cells were incubated in a humidified atmosphere of 5% CO₂/95% air at 37°C.

Stable expression of mito-roGFP2-Orp1 in H1975 cells

H1975 cells stably expressing mito-roGFP2-Orp1 were established by retroviral transduction. Briefly, Phoenix-AMPHO cells were transfected with pLPCX/mito-roGFP2-Orp1 (encoding the roGFP2-Orp1 probe with an

N-terminal mitochondrial targeting sequence) by the calcium phosphate method. After 6 hours of transfection, cells were washed twice with PBS and transferred to fresh medium. After 24 and 48 hours of transfection, supernatant was collected and passed through a 0.22- μ m filter. H1975 cells (seeded at 2.7 × 10⁵ cells per well in a six-well plate for 24 hours before each experiment) were incubated with the virus-containing supernatant supplemented with Polybrene (4 μ g/ml) for 24 hours at 37°C in a 5% CO₂ atmosphere. Cells were then grown in medium containing puromycin (0.5 μ g/ml) for several days. A highly fluorescent cell population (~6% of overall population) was selected by flow cytometry (FACSAria). Collected cells were expanded in the medium containing puromycin (0.5 μ g/ml) and gentamycin (50 μ g/ml).

Subcellular localization of mito-roGFP2-Orp1

Targeting of mito-roGFP2-Orp1 to mitochondria was confirmed by colocalization with TMR (Molecular Probes). Cells placed in cell culture dishes (FluoroDish, World Precision Instruments) were washed twice with Dulbecco's PBS (Invitrogen) and incubated with TMR in Hanks' balanced salt solution (Invitrogen) for 20 min at 37°C. roGFP2 fluorescence was excited with the 488-nm laser line and TMR fluorescence with the 543-nm laser line on a Zeiss LSM 710 ConfoCor 3 microscope equipped with a Plan-Apochromat 63×/1.40 NA (numerical aperture) DIC (differential interference contrast) oil immersion objective.

In vitro characterization of H1975 cells expressing mito-roGFP2-Orp1

H1975 cells expressing mito-roGFP2-Orp1 (4×10^4) in 400 µl of RPMI/ 10% FBS/25 mM Hepes were seeded into the wells of a Lab-Tek Chamber Slide (Fisher Scientific GmbH) 1 day before the experiment. Images were obtained with a Zeiss LSM 710 ConfoCor 3 microscope equipped with an EC Plan N DICI $40 \times /1.3$ NA objective (oil immersion) and a ZEN software. roGFP2 fluorescence was excited sequentially at 405 and 488 nm (line by line) followed by the detection of the emission through the 500- to 550-nm bandpass filter. Real-time measurements were conducted in time series mode under 5% CO₂ at 37°C. After three 15-s intervals, 200 µl of medium containing the compound of interest (H_2O_2 , rotenone, or antimycin A; at 2× final concentration) was added to the cells. Subsequent images were obtained every 15 s.

Animal experiments

Animal experiments were conducted according to local, national, and European Union ethical guidelines and approved by local regulatory authorities.

Xenograft experiments

Five-week-old female NMRI (Naval Medical Research Institute) (nu/nu) mice (Charles River Laboratories) were used for xenografting. After 1 week of acclimatization to individually ventilated cages, Kliba chow 3307 and water ad libitum, 5×10^6 H1975 cells expressing mitoroGFP2-Orp1 were injected subcutaneously. Tumors were allowed to grow up to a size of 15 mm in one diameter, followed by embedding into Tissue-TEK OCT (optimal cutting temperature) compound and snap-freezing in isopentane/liquid nitrogen before storage at -80° C.

Preparation of recombinant adenovirus

Adenovirus expressing mito-roGFP2-Orp1 was generated using a modified pAd-BLOCK-iT vector system (Invitrogen). The mito-roGFP2-Orp1 coding sequence was subcloned into a pENTR entry vector modified to express the probe under control of the CMV (cytomegalovirus) promoter, followed by integration into pAd/BLOCK-iT-DEST. Adenoviruses expressing

mito-roGFP2-Orp1 were produced using the BLOCK-iT Adenoviral RNAi Expression System (Invitrogen) according to the manufacturer's instructions and purified by cesium chloride gradient (28).

In vivo gene transfer and induction of liver inflammation

Male C57BL/6 mice (Charles River Laboratories) were maintained on a 12-hour light-dark cycle with regular unrestricted diet. After 7 days, 2 \times 10^9 plaque-forming units of adenovirus were administered by tail vein injection. After another week, mice were subjected to the following treatments: intraperitoneal injection of 1 μg of recombinant mouse TNF α (410-MT, R&D Systems) and lipopolysaccharide (20 mg/kg) (055:B5) (L4524, Sigma-Aldrich) and intravenous injection of concanavalin A (40 mg/kg) (L7647, Sigma-Aldrich). PBS was injected as vehicle treatment. Mice were sacrificed and analyzed 8 hours after the injection of inflammatory mediators.

Generation of transgenic mice

The generation of mice expressing mito-Grx1-roGFP2 under control of the *Thy1* promoter has been described previously (8). To generate mito-roGFP2-Orp1-expressing mice, roGFP2-Orp1 with a cyclooxygenase 8 (COX8) mitochondrial targeting sequence (*Neurospora crassa*) was cloned into a modified version of the targeting vector pROSA26-1 (29) (a gift from M. Schmidt-Supprian) using Asc I and Sma I restriction sites. The resulting targeting vector contains a *CAG* promoter, a loxP-flanked neo^r-stop cassette, the COX8-roGFP2-Orp1 construct, and a polyadenylation sequence (pROSA26-CAG-loxP-Stop-loxP-AscI-COX8-roGFP2-Orp1-SmaI-polyA). Electroporated JM8.A3 embryonic stem (ES) cells (30) were selected with neomycin, and positive clones were microinjected into C57BL/6N blastocysts and further processed as described by Pettitt and colleagues (30). Chimeric mice were bred for homozygous transgene insertion, crossed with CMV-Cre mice, and then selected for homozygous deletion of the stop cassette.

Preparation of adult murine tissue or tumor sections

Harvested tissues were embedded in Tissue-Tek OCT compound and snap-frozen in isopentane/liquid nitrogen before storage at -80°C. Embedded tissues were warmed to -20°C (brain tissue) or to -25°C (other tissues), cryosectioned into 14-µm slices with a cryotome (Leica CM3050), and mounted onto Superfrost Plus slides (Fisher Scientific GmbH). For sections further processed with chemicals, the chemicals were applied immediately after mounting. To induce maximal probe oxidation or reduction, sections were incubated for 10 min at 4°C with 50 µl of PBS (10.1 mM NaHPO₄, 1.8 mM KH₂PO₄, 136.8 mM NaCl, 2.7 mM KCl) containing 1 mM DA or 10 or 20 mM DTT, respectively, before NEM treatment. To preserve the endogenous redox state, sections were immediately incubated with 80 to 100 µl of PBS containing 50 mM NEM (E3876, Sigma-Aldrich) for 10 min at 4°C followed by fixation in 4% PFA in PBS containing 1 μM TO-PRO-3 (using 0.1% dimethyl sulfoxide as a co-solvent) (T3605, Invitrogen) for 15 min at ambient temperature. PFA was washed out twice with ice-cold PBS for 5 min. Sections were then mounted in Mowiol mounting medium [17% (w/w) Mowiol 4-88 in PBS/glycerol (2:1, v/v)] and kept at 4°C until use.

Immunofluorescence

To detect CD11b, after the fixation step (4% PFA in PBS), sections were washed twice with ice-cold PBS for 5 min and immediately incubated for 60 min in blocking buffer [5% normal goat serum (5425, Cell Signaling Technology) in PBS]. Sections were subsequently incubated with an antibody against CD11b conjugated to Alexa Fluor 594, which was diluted (1:1500) in PBS with 1% bovine serum albumin (BSA). Sections were

incubated overnight at 4°C in a humid light-tight box. Sections were washed three times with PBS and mounted using ProLong Gold Antifade Reagent (8961, Cell Signaling Technology). Microscopy images were taken within 24 hours.

To detect MnSOD (manganese superoxide dismutase), livers were fixed overnight with 4% PFA immediately after excision. Sections (50-µm thickness) prepared by vibratome were rinsed three times with ice-cold PBS for 5 min and incubated for 60 min in blocking buffer (5% normal goat serum and 0.25% Triton X-100 in PBS) at room temperature. Sections were subsequently incubated with an antibody against MnSOD (ADI-SOD-110, StressGen) in an antibody dilution buffer (1% BSA and 0.25% Triton X-100 in PBS) for 20 hours at 4°C. Sections were washed three times in PBS for 5 min and incubated in antibody dilution buffer with a secondary antibody against rabbit immunoglobulin G conjugated to Alexa Fluor 594 (A11012, Invitrogen) (1:300) for 2 hours at room temperature in the dark. Sections were incubated in PBS containing 0.5 µM TO-PRO-3 for 20 min, rinsed three times in PBS for 5 min, and mounted in Mowiol mounting medium.

Starvation

Mice were maintained on a 12-hour light-dark cycle in a temperaturecontrolled barrier facility, with free access to water and food. To examine the effects of fasting, 12-week-old female mice (mito-roGFP2-Orp1expressing or controls) were fasted for 22 to 24 hours or fed ad libitum. After this period, the gastrocnemius and soleus muscles were dissected, promptly embedded into Tissue-Tek OCT compound, and snap-frozen in isopentane/liquid nitrogen before storage at -80°C. Sections were processed as follows: muscle sections were incubated with 50 µl of PBS or PBS containing 50 mM NEM for 10 min at 4°C followed by fixation in 4% PFA in PBS for 30 min at room temperature. PFA was rinsed twice with ice-cold PBS for 10 min. Sections were then mounted in Mowiol mounting medium [17% (w/w) Mowiol 4-88 in PBS/glycerol (2:1, v/v)] and kept at 4°C until use. Microscopy images were taken within 24 hours after sectioning. Mice lacking biosensor expression (ROSA26/CAG-stop^{fl}mito-roGFP2-Orp1 with intact stop cassette) were used as autofluorescence background controls.

Preparation of embryonic tissue sections

At E12.5, embryos were collected, immediately immersed in PBS containing freshly dissolved NEM (100 mM), and incubated for 1.5 hours at 4°C. Embryos were then fixed in 4% PFA in PBS (pH 7.4) plus 100 mM NEM for 1.5 hours at room temperature. Embryos were washed two times in PBS for 10 min, embedded in Tissue-Tek OCT compound, and snapfrozen in isopentane/liquid nitrogen before storage at -80°C. The embryos were oriented to obtain a longitudinal section of the whole animal. At the day of the experiment, the samples were removed from -80°C and kept at -20°C for 1 hour before sectioning. Sections of 14-µm thickness were cut by cryostat, mounted on Superfrost Plus slides (Fisher Scientific GmbH), and dried for 5 min at room temperature. Sections were then mounted in Mowiol mounting medium and kept at 4°C until use. Microscopy images were taken within 24 hours after sectioning.

Image acquisition and image acquisition controls

Guidelines for the use of roGFP2-based redox probes, including microscopy settings and image analysis, have been provided previously (31, 32). In general, fluorescence images were acquired frame by frame by measuring emission at 520 to 540 nm and exciting sequentially with the 405- and 488-nm laser lines. For each animal, at least two images were taken from one or more sections. For starvation experiments, images were acquired using a 40× objective. Tumor, coronal hippocampus, liver, and

embryo images were acquired with a 20× objective on a Leica TCS SP5 inverted confocal microscope using automated tile scanning with 10% overlap between individual images. To control for autofluorescence in tissue sections, we used two approaches. First, control images were taken from tissues lacking biosensor expression (*ROSA26*/CAG-stop^{fl}-mitoroGFP2-Orp1 mice with intact stop cassette or mice injected with PBS instead of adenovirus). These tissues were treated in the same way, and resulting images were used as general autofluorescence background controls. Second, for every sample, an image was acquired with excitation at 405 nm and emission at 460 nm. The resulting autofluorescence image was used for adjusting the background subtraction threshold. Autofluorescence controls were also applied to samples from the developing fetal liver to detect potential autofluorescence of developing blood cells, which showed very weak autofluorescence at all emission wavelengths.

Image processing

In brief, raw image data of the 405- and 488-nm laser lines were exported to ImageJ as 16-bit TIFFs for further analysis. After conversion to 32-bit images, upper and lower thresholds were set for both images to remove background fluorescence and overexposed pixels. Ratio images were created by dividing the 405-nm image by the corresponding 488-nm image pixel by pixel. For visualization of the ratiometric images, the ImageJ lookup table "Fire" was used. For additional quality control, representative images were subjected to detailed inspection and computational analysis as described previously for *Drosophila* tissues (32).

Data representation and statistics

Data are represented as either normalized fluorescence ratios (405/488 nm) or as OxD_{roGFP2}, as box-whisker plot, dot plot, or bar chart. The fluorescence intensity ratio is the primary observable. Raw ratio values depend on the specific experimental conditions (instrument settings) and do not have absolute meaning. They cannot be compared between different experiments unless they are either calibrated relative to both maximum and minimum ratios (formally corresponding to the conversion to OxD) or at least normalized to either the maximum or minimum ratio (labeled "normalized ratio" in our figures). The 405/488-nm raw ratio values were normalized by setting the fully oxidized state (DA control) to 1 (that is, $R_{\text{norm}} = R_{\text{obs}}/R_{\text{ox}}$). In most experiments, fully oxidized (DA) and fully reduced (DTT) samples were prepared to allow calculation of the degree of probe oxidation. The OxD is the ratio of the number of oxidized molecules to the total number of molecules $(OxD_{roGFP2} = [roGFP2_{ox}])$ ([roGFP2_{red}] + [roGFP2_{ox}])). The conversion of raw fluorescence intensities to OxD values was done as previously described (33). In our figures, OxD is expressed as a percentage. In box-whisker plots, data represent median values with a box for the interquartile range and whiskers for the 5th/95th percentiles. Bar diagrams represent normalized ratios as means \pm SEM. In single-cell analyses, 30 cells per sample were randomly collected as individual regions of interests, and measurements were represented as dot plot. The sample size (n) represents the number of samples used for statistics. Student's t test was used for binary comparisons. Statistical significance was defined as *P < 0.05, **P < 0.01, and ***P < 0.001.

SUPPLEMENTARY MATERIALS

www.sciencesignaling.org/cgi/content/full/9/419/rs1/DC1

- Fig. S1. Responsiveness of mito-roGFP2-Orp1 within tumor tissue sections.
- Fig. S2. Characterization of the mito-roGFP2-Orp1 redox state in liver cryosections.
- Fig. S3. The effect of inflammation-induced injury on the redox state of liver tissue.
- Fig. S4. Characterization of the roGFP2 redox state on cryosections from mouse brain.
- Fig. S5. Analysis of mito-roGFP2-Orp1 transgenic mouse embryos.
- Fig. S6. Analysis of muscle sections from mito-roGFP2-Orp1 transgenic mice.

REFERENCES AND NOTES

- M. Schieber, N. S. Chandel, ROS function in redox signaling and oxidative stress. Curr. Biol. 24, R453–R462 (2014).
- M. Ristow, Unraveling the truth about antioxidants: Mitohormesis explains ROS-induced health benefits. Nat. Med. 20, 709–711 (2014).
- 3. J. Yun, T. Finkel, Mitohormesis. Cell Metab. 19, 757-766 (2014).
- M. Gutscher, M. C. Sobotta, G. H. Wabnitz, S. Ballikaya, A. J. Meyer, Y. Samstag, T. P. Dick, Proximity-based protein thiol oxidation by H₂O₂-scavenging peroxidases. *J. Biol. Chem.* 284, 31532–31540 (2009).
- V. V. Belousov, A. F. Fradkov, K. A. Lukyanov, D. B. Staroverov, K. S. Shakhbazov, A. V. Terskikh, S. Lukyanov, Genetically encoded fluorescent indicator for intracellular hydrogen peroxide. *Nat. Methods* 3, 281–286 (2006).
- M. Gutscher, A.-L. Pauleau, L. Marty, T. Brach, G. H. Wabnitz, Y. Samstag, A. J. Meyer, T. P. Dick, Real-time imaging of the intracellular glutathione redox potential. *Nat. Methods* 5, 553–559 (2008).
- S. C. Albrecht, A. G. Barata, J. Großhans, A. A. Teleman, T. P. Dick, In vivo mapping
 of hydrogen peroxide and oxidized glutathione reveals chemical and regional specificity
 of redox homeostasis. *Cell Metab.* 14, 819–829 (2011).
- M. O. Breckwoldt, F. M. J. Pfister, P. M. Bradley, P. Marinković, P. R. Williams, M. S. Brill, B. Plomer, A. Schmalz, D. K. St Clair, R. Naumann, O. Griesbeck, M. Schwarzländer, L. Godinho, F. M. Bareyre, T. P. Dick, M. Kerschensteiner, T. Misgeld, Multiparametric optical analysis of mitochondrial redox signals during neuronal physiology and pathology in vivo. *Nat. Med.* 20, 555–560 (2014).
- B. Morgan, D. Ezerina, T. N. E. Amoako, J. Riemer, M. Seedorf, T. P. Dick, Multiple glutathione disulfide removal pathways mediate cytosolic redox homeostasis. *Nat. Chem. Biol.* 9, 119–125 (2013).
- M. Schwarzländer, T. P. Dick, A. J. Meyer, B. Morgan, Dissecting redox biology using fluorescent protein sensors. *Antioxid. Redox Signal.* 10.1089/ars.2015.6266 (2015).
- D. Knoefler, M. Thamsen, M. Koniczek, N. J. Niemuth, A.-K. Diederich, U. Jakob, Quantitative in vivo redox sensors uncover oxidative stress as an early event in life. Mol. Cell 47, 767–776 (2012).
- P. Niethammer, C. Grabher, A. T. Look, T. J. Mitchison, A tissue-scale gradient of hydrogen peroxide mediates rapid wound detection in zebrafish. *Nature* 459, 996–999 (2009).
- D. Walter, A. Lier, A. Geiselhart, F. B. Thalheimer, S. Huntscha, M. C. Sobotta, B. Moehrle, D. Brocks, I. Bayindir, P. Kaschutnig, K. Muedder, C. Klein, A. Jauch, T. Schroeder, H. Geiger, T. P. Dick, T. Holland-Letz, P. Schmezer, S. W. Lane, M. A. Rieger, M. A. G. Essers, D. A. Williams, A. Trumpp, M. D. Milsom, Exit from dormancy provokes DNA-damage-induced attrition in haematopoietic stem cells. *Nature* 520, 549–552 (2015).
- E. Owusu-Ansah, U. Banerjee, Reactive oxygen species prime *Drosophila* haematopoietic progenitors for differentiation. *Nature* 461, 537–541 (2009)
- H. Bai, W. Zhang, X.-J. Qin, T. Zhang, H. Wu, J.-Z. Liu, C.-X. Hai, Hydrogen peroxide modulates the proliferation/quiescence switch in the liver during embryonic development and posthepatectomy regeneration. *Antioxid. Redox Signal.* 22, 921–937 (2015).
- H.-P. Guan, J. L. Goldstein, M. S. Brown, G. Liang, Accelerated fatty acid oxidation in muscle averts fasting-induced hepatic steatosis in SJL/J mice. *J. Biol. Chem.* 284, 24644–24652 (2009).
- M. Rahman, M. Mofarrahi, A. S. Kristof, B. Nkengfac, S. Harel, S. N. A. Hussain, Reactive oxygen species regulation of autophagy in skeletal muscles. *Antioxid. Redox Signal.* 20, 443–459 (2014).
- M. Schwarzländer, S. Wagner, Y. G. Ermakova, V. V. Belousov, R. Radi, J. S. Beckman, G. R. Buettner, N. Demaurex, M. R. Duchen, H. J. Forman, M. D. Fricker, D. Gems, A. P. Halestrap, B. Halliwell, U. Jakob, I. G. Johnston, N. S. Jones, D. C. Logan, B. Morgan, F. L. Müller, D. G. Nicholls, S. J. Remington, P. T. Schumacker, C. C. Winterbourn, L. J. Sweetlove, A. J. Meyer, T. P. Dick, M. P. Murphy, The 'mitoflash' probe cpYFP does not respond to superoxide. Nature 514, E12–E14 (2014).
- L. P. Roma, J. Duprez, H. K. Takahashi, P. Gilon, A. Wiederkehr, J.-C. Jonas, Dynamic measurements of mitochondrial hydrogen peroxide concentration and glutathione redox state in rat pancreatic β-cells using ratiometric fluorescent proteins: Confounding effects of pH with HyPer but not roGFP1. *Biochem. J.* 441, 971–978 (2012).
- J. Weller, K. M. Kizina, K. Can, G. Bao, M. Müller, Response properties of the genetically encoded optical H₂O₂ sensor HyPer. Free Radic. Biol. Med. 76, 227–241 (2014).
- D. Ezerina, B. Morgan, T. P. Dick, Imaging dynamic redox processes with genetically encoded probes. J. Mol. Cell. Cardiol. 73, 43–49 (2014).
- M. C. Sobotta, A. G. Barata, U. Schmidt, S. Mueller, G. Millonig, T. P. Dick, Exposing cells to H₂O₂: A quantitative comparison between continuous low-dose and one-time high-dose treatments. Free Radic. Biol. Med. 60, 325–335 (2013).
- M. C. Sobotta, W. Liou, S. Stöcker, D. Talwar, M. Oehler, T. Ruppert, A. N. D. Scharf, T. P. Dick, Peroxiredoxin-2 and STAT3 form a redox relay for H₂O₂ signaling. *Nat. Chem. Biol.* 11, 64–70 (2015).
- D. Trachootham, J. Alexandre, P. Huang, Targeting cancer cells by ROS-mediated mechanisms: A radical therapeutic approach? *Nat. Rev. Drug Discov.* 8, 579–591 (2009).

RESEARCH RESOURCE

- V. I. Sayin, M. X. Ibrahim, E. Larsson, J. A. Nilsson, P. Lindahl, M. O. Bergo, Antioxidants accelerate lung cancer progression in mice. Sci. Transl. Med. 6, 221ra15 (2014).
- K. Le Gal, M. X. Ibrahim, C. Wiel, V. I. Sayin, M. K. Akula, C. Karlsson, M. G. Dalin, L. M. Akyürek, P. Lindahl, J. Nilsson, M. O. Bergo, Antioxidants can increase melanoma metastasis in mice. *Sci. Transl. Med.* 7, 308re8 (2015).
- E. Piskounova, M. Agathocleous, M. M. Murphy, Z. Hu, S. E. Huddlestun, Z. Zhao, A. M. Leitch, T. M. Johnson, R. J. DeBerardinis, S. J. Morrison, Oxidative stress inhibits distant metastasis by human melanoma cells. *Nature* 527, 186–191 (2015).
- T. C. Becker, R. J. Noel, W. S. Coats, A. M. Gómez-Foix, T. Alam, R. D. Gerard, C. B. Newgard, Use of recombinant adenovirus for metabolic engineering of mammalian cells. *Methods Cell Biol.* 43 Pt A. 161–189 (1994).
- P. Soriano, Generalized lacZ expression with the ROSA26 Cre reporter strain. Nat. Genet. 21, 70–71 (1999).
- S. J. Pettitt, Q. Liang, X. Y. Rairdan, J. L. Moran, H. M. Prosser, D. R. Beier, K. C. Lloyd, A. Bradley, W. C. Skarnes, Agouti C57BL/6N embryonic stem cells for mouse genetic resources. *Nat. Methods* 6, 493–495 (2009).
- B. Morgan, M. C. Sobotta, T. P. Dick, Measuring E_{GSH} and H₂O₂ with roGFP2-based redox probes. Free Radic. Biol. Med. 51, 1943–1951 (2011).
- A. G. Barata, T. P. Dick, In vivo imaging of H₂O₂ production in *Drosophila*. Methods Enzymol. 526, 61–82 (2013).
- A. J. Meyer, T. P. Dick, Fluorescent protein-based redox probes. Antioxid. Redox Signal. 13, 621–650 (2010).

Acknowledgments: We thank F. Bestvater and M. Brom for the microscopy support; M. Schmidt-Supprian (Technical University Munich) for the *ROSA26* targeting construct; U. Kloz and F. van der Hoeven for ES cell microinjections; A. Reimann for the adenovirus preparations; T. Hielscher for help with the statistics; and A. Pohl-Arnold, B. Steinbauer, G. Kuntz, A. Zota, and Y. Feuchter for technical assistance. **Funding:** T.P.D. acknowledges funding by the DFG (Deutsche Forschungsgemeinschaft) (SFB1036, SFB938, and SPP1710) and the BMBF (Federal Ministry of Education and Research) (LungSysII). S.H.

is supported by the Helmholtz Cross-Program topic "Metabolic Dysfunction" and the "ICEMED" (Imaging and Curing Environmental Metabolic Diseases) alliance. M.K. was supported by the DFG (EXC 1010, SFB-Tr 128, SPP 1710) and the European Research Council (ERC Grant Agreement no. 310932). T.M. was supported by DFG (EXC 114, EXC 1010, SFB 870, and SPP 1710) and the European Research Council under the European Union's Seventh Framework Program (FP/2007-2013; ERC Grant Agreement no. 616791). Y.F. has been supported by the German Cancer Research Center (DKFZ) Postdoctoral Fellowship Program and the Japan Society for the Promotion of Science. L.P.R. has been supported by a postdoctoral fellowship from the São Paulo Research Foundation (FAPESP) and by the DKFZ visiting scientist program. M.C.S. has been supported by a Ph.D. stipend from the Boehringer Ingelheim Fonds. M.O.B. acknowledges support by a physician-scientist fellowship of the Medical Faculty, University of Heidelberg. Author contributions: Y.F. and T.P.D conceived the project. Y.F. and L.P.R. performed the experiments and analyzed the data; T.P.D., M.C.S., and Y.F. designed and generated R26/mito-roGFP2-Orp1 mice; M.K., M.O.B., G.L., T.M., and T.P.D. generated and characterized Thy1-mito-Grx1-roGFP2 mice; K.M.-D. designed and performed tumor xenograft experiments; Y.F., M.B.D., and S.H. designed and performed adenoviral gene transfer and liver inflammation experiments; A.J.R. coordinated mouse starvation experiments; and Y.F., L.P.R., and T.P.D. wrote the manuscript. Competing interests: The authors declare that they have no competing interests. Data and materials availability: Biosensor constructs used in this study are available from Addgene on the basis of a material transfer agreement.

Submitted 6 September 2015 Accepted 24 February 2016 Final Publication 15 March 2016 10.1126/scisignal.aad3895

Citation: Y. Fujikawa, L. P. Roma, M. C. Sobotta, A. J. Rose, M. B. Diaz, G. Locatelli, M. O. Breckwoldt, T. Misgeld, M. Kerschensteiner, S. Herzig, K. Müller-Decker, T. P. Dick, Mouse redox histology using genetically encoded probes. *Sci. Signal.* **9**, rs1 (2016).



Mouse redox histology using genetically encoded probes Yuuta Fujikawa, Leticia P. Roma, Mirko C. Sobotta, Adam J. Rose, Mauricio Berriel Diaz, Giuseppe Locatelli, Michael O. Breckwoldt, Thomas Misgeld, Martin Kerschensteiner, Stephan Herzig, Karin Müller-Decker and Tobias P. Dick (March 15, 2016)

Science Signaling 9 (419), rs1. [doi: 10.1126/scisignal.aad3895]

The following resources related to this article are available online at http://stke.sciencemag.org.

This information is current as of March 18, 2016.

Article Tools Visit the online version of this article to access the personalization and

article tools:

http://stke.sciencemag.org/content/9/419/rs1

Supplemental "Supplementary Materials"

Materials http://stke.sciencemag.org/content/suppl/2016/03/11/9.419.rs1.DC1

Related Content The editors suggest related resources on *Science*'s sites:

http://stke.sciencemag.org/content/sigtrans/7/310/ra10.full http://stke.sciencemag.org/content/sigtrans/1/43/pl3.full http://stke.sciencemag.org/content/sigtrans/2/90/re7.full http://stke.sciencemag.org/content/sigtrans/4/202/ec341.abstract

http://stke.sciencemag.org/content/sigtrans/2005/289/pe30.full http://stke.sciencemag.org/content/sigtrans/7/319/re1.full

References This article cites 32 articles, 5 of which you can access for free at:

http://stke.sciencemag.org/content/9/419/rs1#BIBL

Permissions Obtain information about reproducing this article:

http://www.sciencemag.org/about/permissions.dtl

Science Signaling (ISSN 1937-9145) is published weekly, except the last December, by the American Association for the Advancement of Science, 1200 New York Avenue, NW, Washington, DC 20005. Copyright 2016 by the American Association for the Advancement of Science; all rights reserved.